The Anharmonic Vibrational Potential and Relaxation Pathways of the Amide I and II Modes of *N*-Methylacetamide†

Lauren P. DeFlores, Ziad Ganim, Sarah F. Ackley, Hoi Sung Chung, and Andrei Tokmakoff*

Department of Chemistry, Massachusetts Institute of Technology, Cambridge, Massachusetts 02139

Received: January 17, 2006; In Final Form: April 28, 2006

We investigate the influence of isotopic substitution and solvation of *N*-methylacetamide (NMA) on anharmonic vibrational coupling and vibrational relaxation of the amide I and amide II modes. Differences in the anharmonic potential of isotopic derivatives of NMA in D_2O and DMSO-d_6 are quantified by extraction of the anharmonic parameters and the transition dipole moment angles from cross-peaks in the two-dimensional infrared (2D-IR) spectra. To interpret the effects of isotopic substitution and solvent interaction on the anharmonic potential, density functional theory and potential energy distribution calculations are performed. It is shown that the origin of anharmonic variation arises from differing local mode contributions to the normal modes of the NMA isotopologues, particularly in amide II. The time domain manifestation of the coupling is the coherent exchange of excitation between amide modes seen as the quantum beats in femtosecond pump−probes. The biphasic behavior of population relaxation of the pump−probe and 2D-IR experiments can be understood by the rapid exchange of strongly coupled modes within the peptide backbone, followed by picosecond dissipation into weakly coupled modes of the bath.

I. Introduction

N-Methylacetamide (NMA) is a widely used model compound for investigations into the physical and chemical properties of the amide group, particularly for the purpose of understanding the behavior of one of many peptide linkages in proteins and peptides. Studies of the amide I vibration of NMA have provided insight for vibrational relaxation pathways within peptides,[1,2] peptide solvation, and peptide−solvent hydrogen bonding interactions.[1,3−9] Vibrational techniques show that polar solvents cause large solvatochromic shifts of the amide I and II modes from the gas phase by stabilizing the ionic resonance structure of NMA.[10] The infrared spectroscopy of the amide I vibration is also of interest for its role in understanding the origin of the sensitivity of protein amide I spectroscopy to secondary structure. Many amide I spectroscopic models are based on coupled amide I oscillators,[1,11] in which NMA is used as a model for the individual sites. Less studied are the couplings between vibrations of the amide group, and their consequences for vibrational relaxation pathways.[1,12] Most descriptions of the vibrational motion in proteins and peptides assume the backbone is described by weakly coupled normal modes. However, little has been done to test such notions, and fundamental questions still remain: What is the inherent anharmonic nature of the amide vibrations? How does this manifest itself in terms of vibrational relaxation processes? How is this influenced by the solvent environment and molecular composition?

The connection between vibrational eigenstates and local atomic displacements provides a direct link from spectroscopic observables to the structure of the protein and peptide backbone. Uniformly, the analysis of NMA and protein vibrations is treated in a harmonic basis, a largely untested assumption that the normal modes are only weakly anharmonic and show negligible coupling. Ab initio calculations of NMA in the gas phase and condensed phase have been used to describe the composition of the spectroscopically observable normal modes in a local, or atomic, mode picture,[10,13−15] addressing the role of anharmonicity through various frequency scaling techniques.[16−18] Similarly, NMA experimental studies are interpreted with an amide normal mode picture whose coordinates may vary with different isotopic species,[14,19−21] but anharmonicity of the potential remains largely untested.[22] Some theoretical efforts have been made toward calculating protein vibrational spectroscopy directly from anharmonic potential energy surfaces,[13,23,24] and these studies argue that harmonic force fields are inadequate to describe their spectroscopy. In recent work, Hayashi and co-workers have developed a detailed density functional theory (DFT) electrostatic map for predicting the fundamental and combination bands of many amide modes including electrostatic-induced solvent effects.[25] In the same spirit of these calculations, to appropriately capture intramolecular dynamics and energy flow within the vibrational modes, experimental techniques sensitive to anharmonic properties of a system are required.

In this paper, we examine the anharmonic nature of amide I and II vibrations of NMA using two-dimensional infrared (2D-IR) spectroscopy, a technique inherently sensitive to the anharmonic vibrational potential of the molecule and ultrafast vibrational relaxation. 2D-IR is a femtosecond Fourier transform spectroscopy, which characterizes how vibrational excitation of a mode at frequency ω_1 evolves and is detected in a mode at frequency ω_3. Cross-peaks in a 2D-IR spectrum are an indication of coupled vibrations, and the pattern of peaks in a 2D-IR spectrum can be used to characterize their anharmonic potential.[26,27] 2D-IR spectra acquired as a function of waiting time τ_2 between excitation and detection allow for vibrational relaxation pathways to be unraveled.[28] Here we quantify the amide I/amide II anharmonic coupling strength, the projection angle between their transition dipole moments, and explore pathways for energy relaxation through the use of pump−probe

† Part of the special issue "Robert J. Silbey Festschrift".

10.1021/jp0603334 CCC: $33.50
Published on Web 06/09/2006

and transient 2D-IR experiments. Specifically, these experiments explore the role of solvent and isotopic labeling of NMA on these properties, finding that both of these variables introduce important effects. We will emphasize the need for more explicit models that account for anharmonic coupling that can capture more appropriate dynamics in the protein backbone.

II. Experimental Section

Absorptive two-dimensional infrared spectra were acquired as described in detail elsewhere.[27] Briefly, the Fourier transform 2D-IR experiments were performed with pulsed mid-IR radiation derived from an amplified Ti:sapphire pumped optical parametric amplifier. The pulse spectrum was tuned such that the $\sim$185 cm^{-1} bandwidth (fwhm) is centered to cover both the fundamental ($\upsilon = 0 \rightarrow 1$) and anharmonically shifted ($\upsilon = 1 \rightarrow 2$) overtones of both the amide I and amide II modes of NMA. Three femtosecond pulses sequentially drive the resonant transitions, giving rise to a radiated signal that is heterodyne-detected through spectral interferometry with a local oscillator pulse. A 2D spectrum is obtained from a signal acquired as a function of initial pulse delay τ_1 and detection frequency ω_3 by numerically Fourier transforming with respect to τ_1. The absorptive 2D-IR spectrum is obtained from a sum of rephasing ($k_R = -k_1 + k_2 + k_3$) and nonrephasing ($k_{NR} = k_1 - k_2 + k_3$) 2D spectra. The polarization of the mid-IR pulses was controlled with pairs of $\lambda/2$ waveplates and wire-grid polarizers. Polarization-selective 2D-IR experiments were performed in the parallel (ZZZZ) and perpendicular (ZZYY) geometries, and magic angle spectra were reconstructed for each by summing ZZZZ + 2·ZZYY. For relaxation studies, diagonal and cross-peaks for the absolute-value magic angle rephasing spectra are integrated for multiple spectra acquired as a function of delay time τ_2 between excitation and detection.

Polarization-selective pump−probe measurements were taken using identical conditions as the 2D-IR experiments, by spectrally dispersing the transmitted probe pulse onto an array detector. Dispersed pump−probe spectra are used to phase the 2D-IR spectra. Also, pump−probe transient signals are detected as a function of delay τ_2 at the amide I and II fundamental transition frequency. Signals are acquired for the parallel and perpendicular polarizations, and the magic-angle pump−probe is reconstructed for each.

All chemicals were purchased from Aldrich and used without further purification. *N*-Methylacetamide-d_7 (NMA-d_7) and *N*-methylacetamide-h_7 (NMA-h_7) were dissolved in D_2O, dimethyl-d_6 sulfoxide (DMSO-d_6), and chloroform-d_1 ($CDCl_3$), and held in a CaF_2 sample cell with a 50 μm spacer. Only in the case of NMA-h_7 prepared in D_2O will the amide hydrogen exchange with the solvent giving NMA-d_1. Sample concentrations ($\sim$0.10 mM) were chosen to maintain a peak optical density of $\sim$0.4 for the amide I and amide I′ transitions and $\sim$0.1 for the amide II and amide II′. For clarity in the remainder of paper, the conventional amide notation where primes denote deuterated species will be replaced by explicitly defining the isotopic species of NMA with (-h_7, -d_7, -d_1).

III. Results

The FTIR spectra of isotopologues of NMA in DMSO-d_6, $CDCl_3$, and D_2O are given in Figure 1. Solvation and isotope labeling strongly dictate the vibrational frequencies, intensities, and line widths of the linear spectrum. The amide I vibration red shifts with increasing interaction and polarity of solvent and the amide II vibration blue shifts correspondingly from the gas-phase values. The anticorrelated frequency shifts can be understood as an increased stabilization of the resonance form of NMA by polar solvents.[10,14] The lengthening of the carbonyl bond in the resonance structure reduces the vibrational frequency of the amide I mode while shortening the CN bond and inducing a blue shift of the amide II mode.

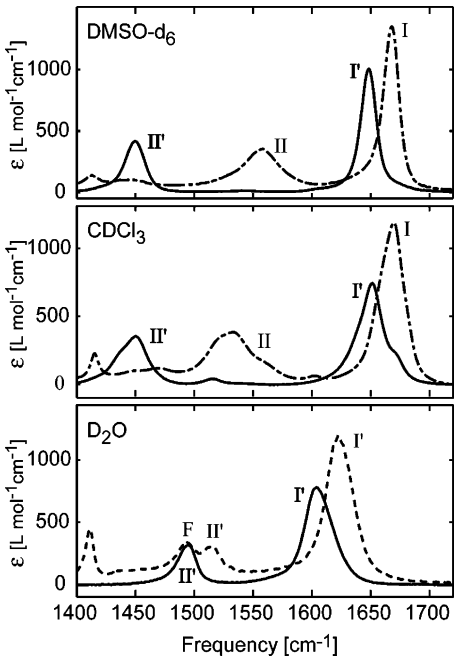

Figure 1. FTIR spectra of NMA-h_7 (dot−dashed), NMA-d_7 (solid), and NMA-d_1 (dashed) in DMSO-d_6, $CDCl_3$, and D_2O. Prime denotes amide vibration with a deuterated amide group.

Labeling the amide hydrogen weakly red shifts the amide I and strongly red shifts the amide II band due to the different contribution of ND in-plane bending (ib). The effect of methyl group deuteration, seen by comparing NMA-d_7 in D_2O with NMA-d_1 in D_2O, is to red shift both amide I and II transitions. This is a result of the methyl deformation contribution to these modes. An interesting feature seen in the NMA-d_1/D_2O spectrum is the presence of the amide II doublet between 1492 and 1514 cm^{-1}. The doublet arises from mixing of a combination band of low-energy backbone modes with the amide II vibration (1514 cm^{-1}), giving rise to a Fermi resonance at 1492 cm^{-1}.[20] The Fermi resonance is not seen in other spectra in which the splitting may be small and only appear as a shoulder on the amide II peak. This may be the case for NMA in $CDCl_3$ where the amide II region appears as overlapping resonances.

To further examine the effects of solvent and isotopes on the vibrational spectrum of NMA, the left column in Figure 2 shows polarization selective 2D-IR surfaces of NMA-d_7 in D_2O (NMA-d_7/D_2O) and NMA-h_7 in DMSO-d_6 (NMA-h_7/DMSO). In all spectra we observe amide I and II diagonal peaks and cross-peaks, and each appears as an oppositely signed doublet. The diagonal features in the 2D-IR spectrum provide information about the nuclear potential of a single vibrational coordinate, here the amide I and II modes. The positive and negative peaks along the diagonal arise from ground-state bleach and excited-state absorption, respectively. The splitting of the doublet along ω_3 gives the difference between the fundamental and overtone transitions and is therefore a measure of the diagonal anharmonicity. Ellipticity or diagonal elongation of the peak, seen clearly for the diagonal amide I peak of NMA-d_7/D_2O, is an indication of the inhomogeneous broadening. This arises from variation of local solvent environments and their dynamics and is discussed in detail elsewhere.[29] Cross-peaks reflect the case

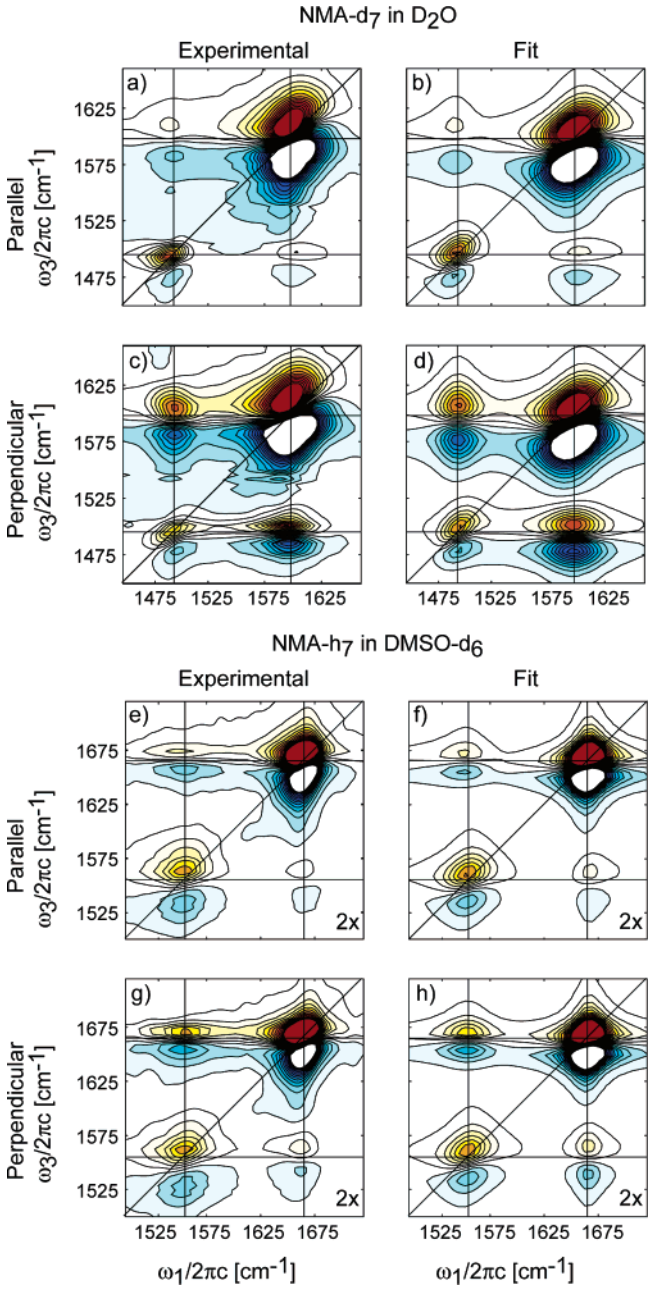

Figure 2. Experimental absorptive 2D-IR spectrum of NMA-d_7/D_2O obtained at $\tau_2 = 80$ fs for parallel (a) and perpendicular (c) polarization and for NMA-h_7/DMSO (e, g). Corresponding fits, (b, d) and (f, h) respectively, are plotted to their right. For each normalized amide I spectrum, 26 equally spaced contours are plotted from ±60% for NMA-d_7/D_2O and from ±30% for NMA-h_7/DMSO. The fit parameters of NMA-d_7/D_2O for the six level system are $\omega_{AI'} = 1598$ cm^{-1}, $\omega_{AII'} = 1495$ cm^{-1}, $\Delta_{AI'} = 15$ cm^{-1}, $\Delta_{AII'} = 11$ cm^{-1}, $\Delta_{AI',AII'} = 11$ cm^{-1}, $\mu_{AI'} = 1$, $\mu_{AII'} = 0.58$, $\mu_{2AI',AI'} = 1.51$ (1.41), $\mu_{2AII',AII'} = 0.68$ (0.82), $\mu_{AI',AII'} = 1.0$ (1.0), $\mu_{AII',\ AI'} = 0.58$ (0.58), and $\Theta = 75°$. For NMA-h_7/DMSO the fit parameters are $\omega_{AI} = 1665$ cm^{-1}, $\omega_{AII} = 1555$ cm^{-1}, $\Delta_{AI} = 12$ cm^{-1}, $\Delta_{AII} = 10$ cm^{-1}, $\Delta_{AI,AII} = 3.8$ cm^{-1}, $\mu_{AI} = 1$, $\mu_{AII} = 0.84$, $\mu_{2AI,AI} = 1.41$ (1.41), $\mu_{2AII,AII} = 1.09$ (1.19), $\mu_{AI,AII} = 0.98$ (1.0), $\mu_{AII,AI} = 0.84$ (0.84), and $\Theta = 40°$. ω is the vibrational frequency, Δ is the anharmonicity, and μ is the transition moment amplitude. Harmonic scaling values are given by parentheses.

where excitation of one resonance influences another transition, and arises from couplings between different vibrational coordinates. The splitting of the cross-peaks along ω_3 gives the off-diagonal anharmonicity of the system.[26] However, the interference between these positive and negative features when the splittings are on the order of the line widths impairs the ability to directly infer parameters from the peak spacing without a fitting algorithm.

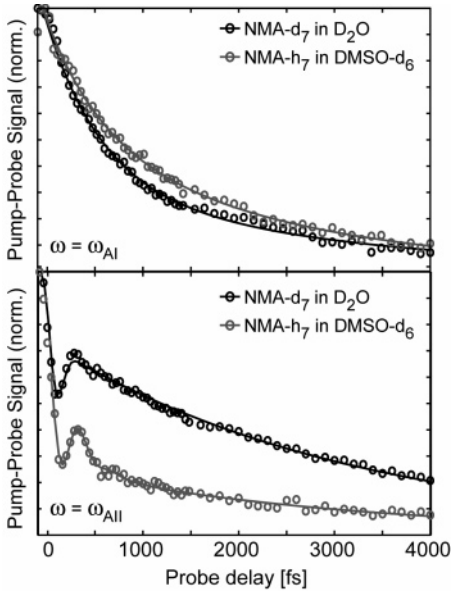

Figure 3. Magic-angle broadband dispersed pump−probes detected at the amide I and II frequencies. Amide I detected signals (top) are shown with a biexponential fit with time scales of 0.38 and 2.1 ps for NMA-d_7/D_2O and 0.43 and 2.1 ps for NMA-h_7/DMSO. The amide II detected signals (bottom) are shown with a fit to a damped cosine plus biexponential. The beats have a period of 0.38 ps and damp with time scales of approximately 0.15 and 0.30 ps for NMA-d_7/D_2O and NMA-h_7/DMSO. The long time tails of are 5.2 and 3.3 ps for the respective systems.

Transition dipole moment magnitudes are reflected in the intensities of the eight-peak structure of the 2D spectrum, with diagonal peaks scaling roughly as the fourth power of the transition moment and cross-peaks scaling as the second power in each of the transitions involved. The projection angle between transition moments is reflected in the variation of cross-peak amplitudes in the parallel and crossed spectra. Nonharmonic scaling of the $v = 0 \rightarrow 1$ and $v = 1 \rightarrow 2$ transition dipole moments arises predominately from the presence of electrical anharmonicity, the nonlinear expansion of the dipole moment in the normal mode coordinate.[30] This can be seen by comparing intensities of oppositely signed peaks referring to the fundamental and overtone transitions.[26] Electrical anharmonicity is apparent in these systems predominately in the amide II vibration.

The presence of cross-peaks in the 2D-IR spectrum is a direct indication of coupling between amide I and II modes. In the time domain, this coherent exchange of vibrational excitation manifests itself as a quantum beat at the Rabi frequency (or the frequency splitting between eigenstates). Figure 3 shows magic-angle dispersed pump probes of NMA-h_7/DMSO and NMA-d_7/D_2O detected at the amide I and II fundamental frequencies. Similar to previous studies performed with only amide I excitation,[1,3] the pump−probe detected at the amide I frequency exhibits a biphasic relaxation whose origin is not understood in detail. The amide II pump−probe shows distinctive beats indicative of coherent exchange between modes. The damping of the quantum beats indicates the loss of coherence of the amide I−II energy exchange process, as a result of either vibrational relaxation to dark states or solvent-induced dephasing. The common longer tail seen in the relaxation at both frequencies suggests a slower relaxation to the bath (solute or solvent) following exchange between amide modes.

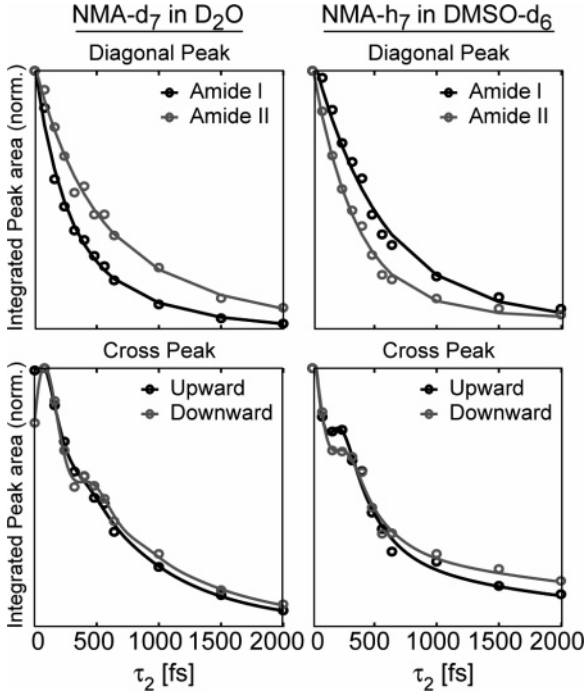

Figure 4. Integrated resonances of absolute value rephasing spectrum along τ_2 are plotted for the diagonal and cross-peak regions of NMA-d_7/D_2O and NMA-h_7/DMSO. Diagonal resonances refer to the amide I and II modes and are fit to biexponentials. The amide II to I (upward) cross-peak and amide I to II (downward) cross-peak are fit to a damped cosine plus biexponential.

To gain a more accurate picture of the vibrational relaxation, the diagonal and cross-peaks of the magic angle absolute value rephasing spectrum are integrated separately as a function of τ_2, shown in Figure 4.[28] These traces show that both diagonal and cross-peaks decay from a maximum at $\tau_2 = 0$ with biphasic relaxation. The diagonal peak amplitudes, which indicate the loss of population from the amide modes, relax faster for amide II than for amide I in the case of NMA-h_7/DMSO, but faster for amide I in the case of NMA-d_7/D_2O. As expected from the light−matter interaction pathways in the rephasing spectrum, beats are only present in the cross-peak time traces.[28] These data are consistent with a strong coupling that exchanges excitation between amide I, amide II, and other peptide modes, followed by a slower dissipation to the bath.

IV. Discussion

A. The Anharmonic Potential and Vibrational Couplings. To quantify the information on the amide I/II anharmonic nuclear potential and projection angle in these systems, the data in Figure 2 were fit using a response function formalism for the amide I and II normal modes of NMA and includes diagonal and off-diagonal anharmonicity.[26,27,31] This model accounts for resonant transitions between six vibrational states: a ground state, one-quantum amide I and II states, doubly excited amide I and II states, and a combination state. The energy gaps between infrared allowed transitions are taken to interact stochastically with a harmonic bath. This system−bath interaction is parametrized using exponential autocorrelation and cross-correlation functions using methods described in detail elsewhere.[29] We also allow for diffusive orientational relaxation, which we have previously characterized for NMA.[3] The orientational response function is a joint probability distribution that reflects sequential interactions of the polarized light fields with transition moments oriented in fixed directions in the molecular frame interlaced with orientational diffusion.[27,32]

The parameters extracted from the 2D spectra describe the anharmonic potential surface for the amide vibrational modes. Parallel and perpendicular experimental data are fit simultaneously using the model described above to extract anharmonicities, orientation, and coupling constants for both NMA-d_7/D_2O and NMA-h_7/DMSO. The results of this fit are shown to the right of the data in Figure 2. The extracted diagonal anharmonicity for amide I/II modes from the fits of the parallel 2D-IR spectra are $\Delta_{AI'} = 15$ cm^{-1} and $\Delta_{AII'} = 11$ cm^{-1}, respectively, for NMA-d_7/D_2O and $\Delta_{AI} = 12$ cm^{-1} and $\Delta_{AII} = 10$ cm^{-1} for NMA-h_7/DMSO. The off-diagonal anharmonicities obtained are $\Delta_{AI',AII'} = 11$ cm^{-1} for NMA-d_7/D_2O and $\Delta_{AI,AII} = 3.8$ cm^{-1} for NMA-h_7/DMSO. The trends of the experimental amide I and II anharmonicities are consistent with the DFT studies of NMA in the condensed and gas phases.[33,34] The anharmonic splitting that we measure for NMA-h_7 compare favorably with those found by Hayashi et al.[34] using a DFT-derived potential with an electrostatic map for solvent effects: $\Delta_{AI} = 14.3$ cm^{-1}, $\Delta_{AII} = 13$ cm^{-1}, and $\Delta_{AI,AII} = 3.1$ cm^{-1}.[34] In the case of NMA-h_7/DMSO, the experimental anharmonic parameters and transition dipole angles are comparable to those found by two-color 2D-IR using two spectrally distinct laser pulses.[12]

We find the observed coupling between the amide I and II vibrational modes to be quite strong. The magnitude and significance of the coupling can be illustrated by interpreting the transition frequencies between the six eigenstates through a model of two bilinearly coupled anharmonic oscillators.[27] Fitting this Hamiltonian to the experimentally determined eigenstates, the bilinear coupling term is determined to be $V_{12} = 39$ and 29 cm^{-1} for NMA-d_7/D_2O and NMA-h_7/DMSO, respectively. Using the obtained zero-order frequencies with peak splitting of $(\omega_1 - \omega_2)/2\pi c = 64$ and 96 cm^{-1}, the Rabi period for exchange between the two vibrations is 0.32 and 0.30 ps in the two respective samples. Comparison of the zero-order frequency peak splitting with the bilinear coupling clearly shows that the weak coupling approximation ($\omega_1 - \omega_2 \gg 4V_{12}$) is not appropriate for the amide I/II system. These findings support the study of Gerber and co-workers, who have argued for the importance of anharmonic effects in protein force fields.[24,35] They find that the anharmonic effects in NMA computed from high-order terms of the potential using the AMBER semiempirical force field are negligible and do not agree well with MP2 *ab initio* calculations or experiment.[13]

B. Vibrational Relaxation. The time domain manifestation of the coherent exchange of vibrational excitation between amide I/II is seen by the quantum beats in the dispersed pump probe of NMA-d_7/D_2O and NMA-h_7/DMSO in Figure 3. These time traces probe the amide I and II modes following abrupt excitation of both amide modes. The amide II pump−probes show clear quantum beating with a period of ∼0.38 ps which is similar to the peak splitting between vibrational eigenstates and consistent with the Rabi periods calculated from the anharmonic potential parameters. From the projection relationship between the dispersed pump−probed and 2D-IR spectrum and the relative amplitudes of peaks in the 2D spectra, one sees that the amide II pump−probe signal is dominated by the cross-peak signal contributions and thereby better reflects the oscillating probability of exchanging vibrational excitation. The beats damp with time scales of approximately 0.15 and 0.30 ps for NMA-d_7/D_2O and NMA-h_7/DMSO, respectively, indicating a very rapid dephasing of the exchange of vibrational excitation either through solvation effects or, more likely, as a result of vibrational relaxation to other amide modes. The amide I traces

exhibit a biphasic relaxation, with a fast time scale less than 0.5 ps and a long time component of roughly 2.1 ps. From the 2D spectrum it is clear that this trace is dominated by signal contributions from the amide I diagonal peak and, therefore, reflect loss of population from the amide I state.

Previous studies have attributed these time scales to the fast amide I fluctuations and/or dissipation of energy through intramolecular vibrational-energy redistribution (IVR) and a slow rearrangement of the hydrogen bonding environment of the solute−solvent system.[1,3] The beats and biphasic relaxation suggest that there is rapid exchange of vibrational excitation not only between the amide I and II bright states but also among other dark amide modes through anharmonic interactions. This would account for the rapid drop in amplitude during the first few hundred femtoseconds and damping of the beats. The longer time relaxation would then be a slower dissipation to the more weakly coupled elements of the bath, presumably in a large part of the solvent. Nonequilibrium molecular dynamics simulations used to study the vibrational energy transfer of peptides in water offer support for this picture.[2] Amide I relaxation dynamics were also found to be biphasic and shown to depend sensitively on the initially prepared state. With pure CO vibrational excitation, the amide I energy shows rapid oscillatory exchange between CO and CN stretches, among other beats, as well as rapid damping. These calculations show early time behaviors in which the excited mode rapidly relaxes into local vibrations through coupling since it is not an eigenstate of the system. Similarly here, our experiments prepare an abrupt excitation of bright amide backbone modes that evolve through coherent and irreversible pathways.

While broad-band pump−probe experiments involve a single abrupt excitation, the 2D-IR data spectrally resolves amide I and amide II frequencies through the Fourier transform of the initial evolution period τ_1. The pump−probe data integrate over several relaxation pathways, whereas the 2D peaks can be interpreted in terms of conditional probabilities of preparing the system at ω_1 and detecting at ω_3. Therefore, detailed information about the system's anharmonic states and their temporal evolution can be extracted from a single waiting-time-dependent 2D experiment. When only the peak position and amplitudes are of interest, comparable information can be obtained from a series of narrow band pump−probe experiments with two independently tunable laser sources.

In Figure 4, vibrational relaxation in these systems is presented by integrating the amplitude of the diagonal and cross-peaks of the 2D spectrum as a function of waiting time. The relaxation of amplitude in all peaks of the magic angle rephasing spectra proceeds from a maximum at $\tau_2 \approx 0$, implying that during the evolution period τ_1, the amide I and II vibrations have already efficiently exchanged excitation. If the coupling were weak between the two modes, the cross-peak amplitude would grow in as population exchanged during τ_2. The amplitude decay of diagonal and cross-peaks is seen to be biphasic with a few-hundred-femtosecond short component and a longer ~1 ps decay for NMA-d_7/D_2O and >2 ps for NMA-h_7/DMSO. These observations are also consistent with rapid exchange between a manifold of strongly coupled modes within the peptide, followed by a slower dissipation from these to the bath—primarily to the solvent. In the case of NMA-h_7/DMSO, the amide II diagonal peak initially relaxes faster (0.35 ps) than the amide I (0.45 ps), suggesting that amide II is more strongly coupled to the other backbone vibrations for NMA-h_7.[1] For NMA-d_7/D_2O the amide I mode relaxes faster (0.21 ps) than amide II (0.38 ps), suggesting a change in intramolecular vibrational-energy redistribution pathway between the two systems. All indications suggest that the fast time scale for vibrational relaxation is intramolecular energy redistribution and that the relaxation process is a property of the peptide unit solely.

Vibrational energy exchange with close lying Fermi resonances and the amide III mode provides energetically favorable relaxation pathways to lower frequency amide modes. Fermi resonances are seen in the spectra of NMA-d_1 in D_2O (Figure 1) and offer direct evidence of anharmonic couplings to lower frequency NMA modes. This conclusion has been drawn previously based on vibrational relaxation data of the amide I mode of NMA-d_1/D_2O.[1] The recent computational study of the amide I, II, III, and A anharmonic potential of NMA-h_7 by Hayashi et al.[34] can be used to argue that the amide III mode is one of the dominant relaxation pathways from amide I/II. If the eigenstates obtained from their DFT calculations for the amide I/III and amide II/III systems are interpreted within the model of coupled anharmonic oscillators described above, the zero-order frequency splitting is determined to be 398 and 150 cm^{-1} with bilinear coupling terms of 12 and 97 cm^{-1}, respectively. These results show the amide II mode can be expected to couple strongly to amide III mode in the case of NMA-h_7.

C. Transition Dipole Orientation and Amide Mode Composition. One of the prominent differences between NMA-d_7/D_2O and NMA-h_7/DMSO is the variation of cross-peak amplitude between parallel and perpendicular polarization data. A comparison of cross-peak intensities in the two spectra gives direct information about the projection angle Θ between the $v = 0 \rightarrow 1$ transition dipole moments of the amide I and II eigenstates.[27,36] The strong enhancement of the cross-peak amplitude for NMA-d_7/D_2O in the perpendicular geometry is an immediate indicator that the projection angle varies considerably between the two species. By fitting the parallel and perpendicular 2D spectra simultaneously to the formalism described above, the projection angles are determined to be 75° for NMA-d_7/D_2O and 40° for NMA-h_7/DMSO.

The variation of the angle and anharmonic coupling between the transition moments raises an important question about the intrinsic nature of normal modes in NMA as a function of solvent and isotope effects. To construct a better picture of the normal modes, DFT calculations using the Gaussian[37] implementation of the B3LYP with the 6-311++G(d,p) basis set were performed to determine the normal modes of NMA-h_7, NMA-d_7, and NMA-d_1 in the gas phase. The MOLVIB[38a] module in CHARMM[38b] was used to compute the potential energy distribution (PED) by projecting the DFT-calculated normal modes onto an internal coordinate system detailed by Pulay et al.[39] The results are summarized in Table 1.

PED analysis of the amide I and II modes in the gas phase indicate a distinct variation in normal mode composition upon isotopic substitution of the amide and methyl groups of NMA. The amide I PED analysis gives the mode composed of 81−86% CO stretch (s) for NMA-h_7, NMA-d_7, and NMA-d_1. All isotopic species have dipole moments for the amide I vibration to be between 12° and 15° off the carbonyl bond, which is consistent with the value of 20° commonly used in the literature.[40] Since methyl deformations and N−H modes contribute weakly to the amide I transition, isotopic effects minimally contribute to the mode composition and transition moment angle. The amide II vibration is cited as being mostly CN s with NH in-plane bend (ib), leading to a transition moment approximately 68° from the NH bond.[40] The mode decomposition of amide II in the gas phase shows drastically different

TABLE 1: Amide I (AI) and Amide II (AII) Transition Frequencies and Transition Dipole Angles for Isotopic Species of NMA in the Gas Phase, D_2O, and DMSO-d_6[a]

		$\omega/2\pi c$ (cm^{-1}) (exptl)	$\omega/2\pi c$ (cm^{-1}) (calcd)	Θ (deg) (exptl)	θ (deg) (calcd)	$\angle$CO−AI (deg) $\angle$CN−AII (deg)	potential energy distribution
Gas Phase							
NMA-h_7	AI	1728[b]	1744		54	13	CO s (81), CCN d (4)
	AII	1500[b]	1559			10	NH ib (42), Me_1 d (22), CN s (19)
NMA-d_1	AI′	1717[b]	1739		54	16	CO s (83), CCN d (4), CN s (4)
	AII′	1440[b]	1517			12	Me_1 d (81), CN s (7)
NMA-d_7	AI′		1733		62	15	CO s (86), CCN d (4)
	AII′		1432			20	CN s (49), ND ib (16), CO ib (9)
D_2O							
NMA-h_7	AI		1655		45	18	CO s (62), CN s (11), Me_2 d (10), NH ib (8), CCN d (5)
	AII		1617			6	NH ib (58), CN_1 s (26)
NMA-d_1	AI′	1623	1650		90	26	CO s (60), CN s (20), Me_2 d (11), CCN d (5)
	AII′	1493	1521			59	Me_1 d (38), CO s (13), CN s (10), ND ib (8), CC s (7), Me_2 d (6)
NMA-d_7	AI′	1604	1634	75	72	24	CO s (70), CN s (18), CCN d (5)
	AII′	1495	1499			39	CN s (45), ND ib (15), CC s (11), CO ib (9), NC s (8), CO s (8)
DMSO-d_6							
NMA-h_7	AI	1668	1679	40	41	11	CO s (63), NH ib (18), Me_2 d (6), CCN d (4), CN s (4)
	AII	1558	1624			−5	NH ib (60), CN s (22), CO s (6)
NMA-d_1	AI′		1667		81	11	CO s (71), CN s (12), Me_2 d (7), CCN d (5)
	AII′		1509			45	Me_1 d (85), CN s (5)
NMA-d_7	AI′	1648	1655		64	19	CO s (78), CN s (10), CCN d (4)
	AII′	1450	1474			27	CN s (49), ND ib (18), NC s (9), CC s (9), CO ib (8)

[a] Experimental frequencies are extracted from FTIR spectra or as indicated. Calculated frequencies are the harmonic normal-mode frequencies from DFT calculations. The amide I−II projection angle Θ is that between the eigenvectors extracted from fits to the 2D-IR spectra, and the calculated angle θ is that between the normal mode coordinates. Also given are the calculated angles of amide I transition moment relative to the CO bond ($\angle$CO−AI) and the amide II transition moment relative to the CN bond ($\angle$CN−AII). Potential energy distribution calculations are given for amide I contributions ≥4% and amide II contributions ≥5%. Mode definitions are defined by: s = stretch, d = deformation, ib = in-plane bend (peptide bond). All methyl motions were combined into a single methyl deformation mode for simplicity and Me_1 is the C terminus and Me_2 is the N terminus methyl. For definitions of internal coordinate system see Pulay et al.[39] [b] Frequencies obtained from Mayne et al.[22]

local mode distributions for the isotopic species. Deuteration of the methyl groups reduces the effective influence of methyl deformation on the amide II vibration therefore localizing the mode to the peptide backbone. This effect is consistent with assumptions made in large protein systems in which the normal modes are localized to their respective peptide unit, where in this study the neighboring side chains are mimicked by heavier methyl capping groups. The remaining isotopologues show different mode composition where NMA-d_1 is dominated by methyl deformations and NMA-h_7 is predominately NH ib. The large variations in projection angles of the gas-phase isotopologues are explained by these differences in the amide II local mode character. The calculated projection angle between the normal mode transition moments, θ, is tabulated in Table 1.

Solute−solvent interactions play a vital role in the amide spectroscopy of proteins and peptides. Prior theoretical[6−8,34,41−43] and experimental studies[1,3,5,9] have concentrated on the influence of solvent motions and hydrogen bonding on NMA's amide I transition frequency. In our prior analysis of the τ_2-dependent amide I 2D-IR line shape, we concluded that the influence of the local hydrogen bonding environment and solvent motions on amide I frequency is well modeled by electrostatic models for the system−bath interaction.[3] Solvatochromic shifts are also observed from FTIR spectra for the amide II mode of NMA (Figure 1 and Table 1), although in this case a blue shift is observed with increasingly strong hydrogen bonding interactions that act to stabilize the zwitterionic form of NMA.

These earlier studies concentrated on the time-dependent amide I energies for the system−solvent interaction. To turn to characterization of the solvation effect on the amide eigenvectors, the DFT calculations and PED analysis of the amide I and II modes were recalculated using an explicit solvent model for the first solvation shell and treating the remaining solvent implicitly. Calculations of NMA-h_7, NMA-d_7, and NMA-d_1 were done for NMA−$(D_2O)_3$ and NMA−DMSO-d_6 clusters, embedded in a dielectric continuum matching the static dielectric constant for each solvent.[10,14,15,44] The coordination of NMA-d_7 to D_2O is through three hydrogen-bonding sites, two on the carbonyl oxygen and one on the ND group of the peptide, and NMA-h_7/DMSO has a single hydrogen-bonding site to the NH.

Upon hydrogen bonding to the solvent, the amide I and II mode compositions show a small change. The amide II mode becomes more delocalized, picking up more backbone stretches and bends. The amide I mode composition in both DMSO-d_6 and D_2O changes from the gas phase similarly, reducing the CO s local mode by approximately 10−15% and increasing the localization of the mode on the CN s. This effect explains the increased coupling of the amide vibrations in NMA-d_7/D_2O in which the amide II is dominated by the CN stretch for fully deuterated NMA. This trend of isotopic effects on the transition moment directions and projection angles of NMA-d_7/D_2O and NMA-h_7/DMSO is pictured in the bottom panel of Figure 5. These values are close to the experimentally determined projection values, although we note that these are not directly comparable, since they are represented in a normal mode basis as opposed to the eigenbasis.

PED calculations strongly suggest that the isotopic substitution of NMA, not solvation, governs the large variations in observed 2D-IR spectral features. For additional comparison of solvation and isotope effects, the 2D-IR polarization-selective spectra were taken for NMA-d_1 in D_2O and NMA-h_7 in $CDCl_3$ and are shown in Figure 6. The large off-diagonal anharmonicity and cross-peak enhancement of the NMA-d_7/D_2O is not seen in the NMA-d_1 in D_2O spectra, which have identical solvation environments. NMA-h_7 in $CDCl_3$ shows similar spectral features to the NMA-h_7/DMSO system. DMSO and $CDCl_3$ have very different solvation characteristics in which DMSO hydrogen bonds to the NH of the amide group and roughly two $CDCl_3$ molecules weakly hydrogen bond to the carbonyl.[3] This clearly

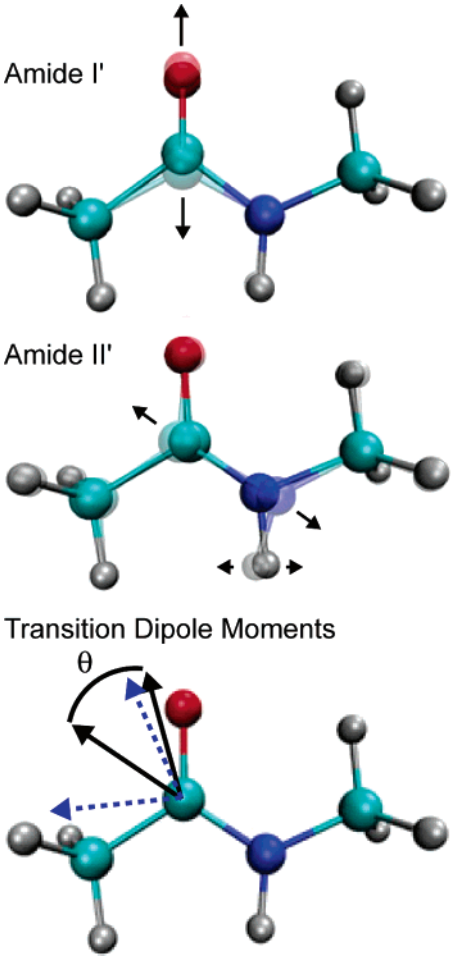

Figure 5. (top, middle) Normal mode displacements of the amide I and II vibrational bands of NMA-d_7 in the gas phase. (bottom) The amide I/II transition dipole angles for NMA-d_7/D_2O (blue dashed arrow) and NMA-h_7 in DMSO-d_7 (black solid arrow) where Θ defines the experimentally determined angle from the polarization 2D-IR spectra given in Table 1.

shows that the isotope effects are dictating the intramolecular coupling and transition moment variation in these samples.

PED analysis of the normal modes has been used to assign Fermi resonances in the NMA vibrational spectra, which provide energetically favorable pathways for vibrational relaxation. For the amide II doublet of NMA-d_1/D_2O, it has been proposed that the 1492 cm^{-1} peak arises from a Fermi resonance between amide II and a combination band of the amide IV and peptide skeletal deformation modes.[20] In the case of NMA-h_7 in $CDCl_3$, the assignment of the somewhat structured and asymmetric resonance at ~1530 cm^{-1} is not possible from FTIR; however, the 2DIR spectrum indicates clearly that this absorption feature involves two overlapping resonances at 1558 and 1532 cm^{-1}. The 2D-IR spectrum of NMA-h_7 in $CDCl_3$ also exhibits strong similarity to the amide II and cross-peak region with that of NMA-d_1/D_2O. The cross-peak enhancement in the perpendicular polarized 2D-IR spectrum is primarily between amide I and II at 1623 and 1514 cm^{-1}, respectively. The similarity between the 2D-IR spectra in Figure 6, showing that the dominant cross-peak to amide I with the shoulder of the 1558 cm^{-1} transition, suggests that this higher energy shoulder is the amide II mode and the 1532 cm^{-1} transition arises from a Fermi resonance.

V. Conclusion

Our study of the effects of solute−solvent interactions and deuteration on the amide I and II vibrational couplings, mode

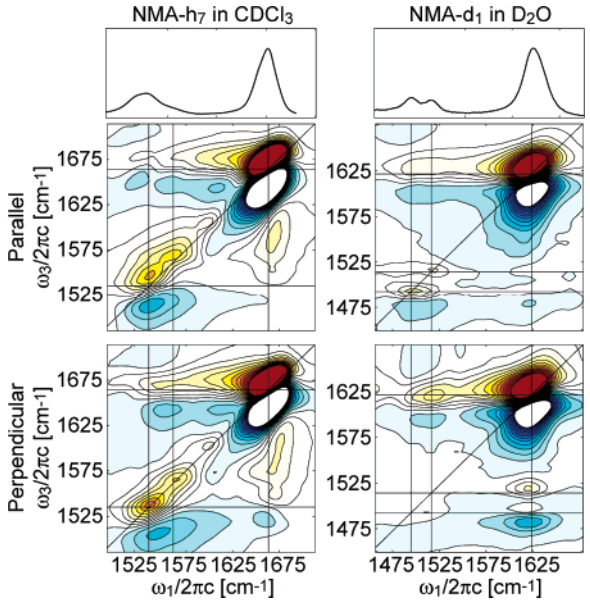

Figure 6. FTIR spectra (top), parallel (middle), and perpendicular (bottom) absorptive 2D-IR spectrum of NMA-h_7 in $CDCl_3$ and NMA-d_1 in D_2O at $\tau_2 = 0$ fs. Twenty-six equally spaced contours are plotted from ±25% for NMA-h_7/$CDCl_3$ and from ±50% for NMA-d_1/D_2O of the normalized amide I spectral amplitude.

composition, and vibrational relaxation for isotopic species of NMA indicates that anharmonicity plays an important role in understanding the structure and energy exchange processes of peptides. The cross-peaks in 2D-IR spectra and quantum beats in pump−probe experiments are indicators of a rapid coherent exchange of energy between these coordinates. Thus, the common picture of weakly coupled normal modes, an assumption within most empirical potentials for biomolecules, does not properly describe the nuclear potential of a peptide linkage. The degree of coupling, mode composition, transition dipole moment orientation, and vibrational relaxation time scales for NMA is governed by the isotopic substitution of the amide and methyl groups, with the most significant effects on the amide II mode. The rapid vibrational relaxation processes observed argue for rapid intramolecular vibrational energy redistribution among a set of coupled peptide backbone modes followed by a slower energy dissipation into weakly coupled vibrations of the peptide and solvent motions. These results also indicate that NMA-h_7 is perhaps the least representative of a peptide group in a protein, due to the relatively light terminal methyl groups. Rather than deuterating the methyls, it may be better to study an amide with more massive terminal groups, for instance *N*-ethylpropionamide.

The consequences of strong couplings could be significant for modeling protein vibrational spectroscopy, particularly for efforts to model the amide I spectroscopy of proteins and understand its sensitivity to secondary structure. Structure-based spectroscopic models of the amide I spectrum are often based on a Hamiltonian formulated in a local mode amide I basis, where amide I oscillators parametrized from NMA interact with one another with through-space and through-bond couplings.[1,11] The magnitudes of the couplings observed here are no less than short-range through-space electrostatic interactions, suggesting that amide I vibrational couplings between bonded peptide groups may originate in their mutual coupling to amide backbone vibrations, such as the amide II. In fact, the importance of through-bond interaction in modeling amide I spectroscopy is already well-known but has to now only been treated by deducing amide I couplings from *ab initio* and DFT calculations

of dipeptides as a function of torsion angles.[11,45,46] Currently there are conflicting accounts of amide II couplings between peptide units, with experiments arguing for negligible coupling[47] and theory arguing for strong interactions.[48] Experiments on amide I and II couplings in dipeptides would help resolve this issue and would offer insight into the elements of a more robust protein spectroscopic model.

Acknowledgment. This work was supported by the National Science Foundation (Grant CHE-0316736). A.T. thanks the David and Lucile Packard Foundation for their fellowship support.

References and Notes

(1) Hamm, P.; Lim, M.; Hochstrasser, R. M. *J. Phys. Chem. B* **1998**, *102*, 6123.

(2) Nguyen, P. H.; Stock, G. *J. Chem. Phys.* **2003**, *119*, 11350.

(3) DeCamp, M. F.; DeFlores, L. P.; McCracken, J. M.; Tokmakoff, A.; Kwac, K.; Cho, M. *J. Phys. Chem. B* **2005**, *109*, 11016.

(4) Rubtsov, I. V.; Kumar, K.; Hochstrasser, R. M. *Chem. Phys. Lett.* **2005**, *402*, 439.

(5) Woutersen, S.; Mu, Y.; Stock, G.; Hamm, P. *Chem. Phys.* **2001**, *266*, 137.

(6) Kwac, K.; Cho, M. *J. Chem. Phys.* **2003**, *119*, 2247.

(7) Schmidt, J. R.; Corcelli, S. A.; Skinner, J. L. *J. Chem. Phys.* **2004**, *121*, 8887.

(8) Bour, P.; Keiderling, T. A. *J. Chem. Phys.* **2003**, *119*, 11253.

(9) Zanni, M. T.; Asplund, M. C.; Hochstrasser, R. M. *J. Chem. Phys.* **2001**, *114*, 4579.

(10) Besley, N. A. *J. Phys. Chem. A* **2004**, *108*, 10794.

(11) Woutersen, S.; Hamm, P. *J. Phys.: Condens. Matter* **2002**, *14*, 1035.

(12) Rubtsov, I. V.; Wang, J.; Hochstrasser, R. M. *Proc. Natl. Acad. Sci. U.S.A.* **2003**, *100*, 5601.

(13) Gregurick, S. K.; Chaban, G. M.; Gerber, R. B. *J. Phys. Chem. A* **2002**, *106*, 8696.

(14) Kubelka, J.; Keideling, T. A. *J. Phys. Chem. A* **2001**, *105*, 10922.

(15) Mirkin, N. G.; Krimm, S. *J. Mol. Struct.* **1996**, *377*, 219.

(16) Scott, A. P.; Radom, L. J. *J. Phys. Chem. A* **1996**, *100*, 16502.

(17) Pulay, P.; Fogarasi, G.; Pongor, G.; Boggs, J. E.; Vargha, A. *J. Am. Chem. Soc.* **1983**, *105*, 7037.

(18) Allen, W. D.; Csaszar, A. G.; Horner, D. A. *J. Am. Chem. Soc.* **1992**, *114*, 6834.

(19) Mix, G.; Schweitzer-Stenner, R.; Asher, S. A. *J. Am. Chem. Soc.* **2000**, *122*, 9028.

(20) Chen, X. G.; Schweitzer-Stenner, R.; Asher, S. A.; Mirkin, N. G.; Krimm, S. *J. Phys. Chem.* **1995**, *99*, 3074.

(21) Torii, H.; Tatsumi, T.; Kanazawa, T.; Tasumi, M. *J. Phys. Chem. B* **1998**, *102*, 309.

(22) Mayne, L. C.; Hudson, B. *J. Phys. Chem.* **1991**, *95*, 2962.

(23) Roitberg, A.; Gerber, R. B.; Elber, R.; Ratner, M. A. *Science* **1995**, *268*, 1319.

(24) Gerber, R. B.; Brauer, B.; Gregurick, S. K.; Chaban, G. M. *PhysChemComm* **2002**, *21*, 142.

(25) Hayashi, T.; Jansen, T. l. C.; Zhuang, W.; Mukamel, S. *J. Phys. Chem. A* **2005**, *109*, 64.

(26) Golonzka, O.; Khalil, M.; Demirdöven, N.; Tokmakoff, A. *Phys. Rev. Lett.* **2001**, *86*, 2154.

(27) Khalil, M.; Demirdoven, N.; Tokmakoff, A. *J. Phys. Chem. A* **2003**, *107*, 5258.

(28) Khalil, M.; Demirdöven, N.; Tokmakoff, A. *J. Chem. Phys.* **2004**, *121*, 362.

(29) Demirdöven, N.; Khalil, M.; Tokmakoff, A. *Phys. Rev. Lett.* **2002**, *89*, 237401.

(30) Khalil, M.; Tokmakoff, A. *Chem. Phys.* **2001**, *266*, 213.

(31) Sung, J.; Silbey, R. J. *J. Chem. Phys.* **2001**, *115*, 9266.

(32) Golonzka, O.; Tokmakoff, A. *J. Chem. Phys.* **2001**, *115*, 297.

(33) Wang, J.; Hochstrasser, R. *J. Phys. Chem. B* **2006**, *110*, 3798.

(34) Hayashi, T.; Zhuang, W.; Mukamel, S. *J. Phys. Chem. A* **2005**, *109*, 9747.

(35) Roitberg, A.; Gerber, R. B.; Elber, R.; Ratner, M. A. *Science* **1995**, *268*, 1319.

(36) Golonzka, O.; Khalil, M.; Demirdöven, N.; Tokmakoff, A. *J. Chem. Phys.* **2001**, *115*, 10814.

(37) Frisch, M. J.; Trucks, G. W.; Schlegel, H. B.; Scuseria, G. E.; Robb, M. A.; Cheeseman, J. R.; Zakrzewski, V. G.; Montgomery, J. A., Jr.; Stratmann, R. E.; Burant, J. C.; Dapprich, S.; Millam, J. M.; Daniels, A. D.; Kudin, K. N.; Strain, M. C.; Farkas, O.; Tomasi, J.; Barone, V.; Cossi, M.; Cammi, R.; Mennucci, B.; Pomelli, C.; Adamo, C.; Clifford, S.; Ochterski, J.; Petersson, G. A.; Ayala, P. Y.; Cui, Q.; Morokuma, K.; Malick, D. K.; Rabuck, A. D.; Raghavachari, K.; Foresman, J. B.; Cioslowski, J.; Ortiz, J. V.; Stefanov, B. B.; Liu, G.; Liashenko, A.; Piskorz, P.; Komaromi, I.; Gomperts, R.; Martin, R. L.; Fox, D. J.; Keith, T.; Al-Laham, M. A.; Peng, C. Y.; Nanayakkara, A.; Gonzalez, C.; Challacombe, M.; Gill, P. M. W.; Johnson, B. G.; Chen, W.; Wong, M. W.; Andres, J. L.; Head-Gordon, M.; Replogle, E. S.; Pople, J. A. *Gaussian 98*; Gaussian, Inc.: Pittsburgh, PA, 1998.

(38) (a) Kuczera, K.; Wiorkiewicz, J. K.; Karplus, M. MOLVIB: Program for the Analysis of Molecular Vibrations; CHARMM; Harvard University, 1993. (b) MacKerell, A. D.; Bashford, D.; Bellott, M.; Dunbrack, R. L.; Evanseck, J. D.; Field, M. J.; Fischer, S.; Gao, J.; Guo, H.; Ha, S.; Joseph-McCarthy, D.; Kuchnir, L.; Kuczera, K.; Lau, F. T. K.; Mattos, C.; Michnick, S.; Ngo, T.; Nguyen, D. T.; Prodhom, B.; Reiher, W. E.; Roux, B.; Schlenkrich, M.; Smith, J. C.; Stote, R.; Straub, J.; Watanabe, M.; Wiorkiewicz-Kuczera, J.; Yin, D.; Karplus, M. *J. Phys. Chem. B* **1998**, *102*, 3586.

(39) Pulay, P.; Fogarasi, G.; Pang, F.; Boggs, J. E. *J. Am. Chem. Soc.* **1979**, *101*, 2550.

(40) Moore, W. H.; Krimm, S. *Biopolymers* **1976**, *15*, 2439.

(41) Bour, P. *J. Chem. Phys.* **2004**, *121*, 7545.

(42) Kwac, K.; Lee, H.; Cho, M. *J. Chem. Phys.* **2004**, *120*, 1477.

(43) Jansen, T. L. C.; Knoester, J. *J. Chem. Phys.*, in press.

(44) Guo, H.; Karplus, M. *J. Phys. Chem.* **1992**, *96*, 7273.

(45) Torii, H.; Tasumi, M. *J. Raman Spectrosc.* **1998**, *29*, 81.

(46) Cha, S.; Ham, S.; Cho, M. *J. Chem. Phys.* **2002**, *117*, 740.

(47) Mikhonin, A. V.; Asher, S. A. *J. Am. Chem. Soc.* **2005**, *109*, 3047.

(48) Moran, A.; Mukamel, S. *Proc. Natl. Acad. Sci. U.S.A.* **2004**, *101*, 506.